Registration in bounded domains for model reduction of parametric conservation laws

Tommaso Taddei, Sapienza University of Rome.

Symposium: *Mathematical and applied aspects of complexity reduction methods*
Paris, Collège de France. June, 2026.

Collaborators: N Barral, A Iollo, J Labatut, I Tifouti (Inria).
Sponsors: AEx Inria, EDF, Onera (Chaire PROVE).

SAPIENZA
UNIVERSITÀ DI ROMA

Objective

Model order reduction (MOR) of parametric systems

MOR methods aim to reduce the *marginal* cost of the solution to the parametric problem: find $u_\mu \in \mathcal{X} \,:\, R_\mu(u_\mu) = 0$.

- $R_\mu : \mathcal{X} \to \mathcal{Y}'$ residual of the equations;
- $\mu \in \mathcal{P}$ vector of model parameters;
- $\mathcal{X}, \mathcal{Y}$ suitable Hilbert spaces defined on the domain Ω;
- $\mathcal{M} := \{u_\mu : \mu \in \mathcal{P}\} \subset \mathcal{X}$ solution set.

MOR methods aim to reduce the *marginal* cost of the solution to the parametric problem: find $u_\mu \in \mathcal{X} \ : \ R_\mu(u_\mu) = 0$.

- $R_\mu : \mathcal{X} \to \mathcal{Y}'$ residual of the equations;
- $\mu \in \mathcal{P}$ vector of model parameters;
- $\mathcal{X}, \mathcal{Y}$ suitable Hilbert spaces defined on the domain Ω;
- $\mathcal{M} := \{u_\mu : \mu \in \mathcal{P}\} \subset \mathcal{X}$ solution set.

Building blocks of MOR techniques

1. HF discretization: determine an high-fidelity (HF) discretization of the problem, $\mathcal{X} \to \mathcal{X}_{\rm hf}, \mathcal{Y} \to \mathcal{Y}_{\rm hf}, u_\mu \to u_\mu^{\rm hf}$.

2. Data compression: find a low-rank representation of the solution field $u_\mu^{\rm hf} \approx \widehat{u}_\mu := Z(\widehat{\alpha}_\mu)$ with $Z : \mathbb{R}^n \to \mathcal{X}_{\rm hf}$, $\widehat{\alpha}_\mu \in \mathbb{R}^n$.

3. ROM formulation: determine a reduced-order model (ROM) for $\mu \mapsto \widehat{\alpha}_\mu$.

Nonlinear approximations (I): inadequacy of linear methods

Traditional MOR methods rely on

- linear approximations, $\widehat{u}_\mu = Z\,\widehat{\alpha}_\mu$, with Z linear operator;

- a single high-fidelity discretization to represent *all* elements of the solution set $\mathcal{M} = \{u_\mu \,:\, \mu \in \mathcal{P}\}$.

Nonlinear approximations (I): inadequacy of linear methods

Traditional MOR methods rely on

- linear approximations, $\widehat{u}_\mu = Z\,\widehat{\alpha}_\mu$, with Z linear operator;

  Linear approximations are inadequate for transport phenomena.

- a single high-fidelity discretization to represent *all* elements of the solution set $\mathcal{M} = \{u_\mu \,:\, \mu \in \mathcal{P}\}$.

  Mesh adaptation is needed to resolve sharp features.

Technical issue: slow decay of Kolmogorov n-width.

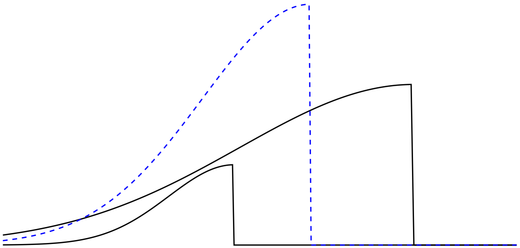

Illustration courtesy of M Zahr (Univ. Notre Dame).

Nonlinear approximations (I): inadequacy of linear methods

Traditional MOR methods rely on

- linear approximations, $\widehat{u}_\mu = Z\,\widehat{\alpha}_\mu$, with Z linear operator;

  Linear approximations are inadequate for transport phenomena.

- a single high-fidelity discretization to represent *all* elements of the solution set $\mathcal{M} = \{u_\mu \,:\, \mu \in \mathcal{P}\}$.

  Mesh adaptation is needed to resolve sharp features.

Technical issue: slow decay of Kolmogorov n-width.

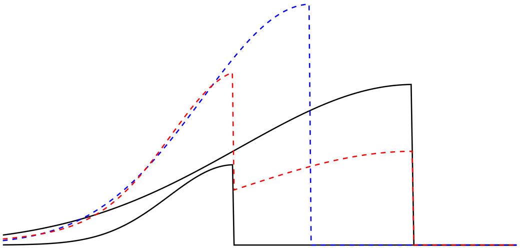

Illustration courtesy of M Zahr (Univ. Notre Dame).

Intuition: in several cases, coherent structures (e.g., shocks) vary smoothly wrt μ.

Lagrangian ansatz: replace the linear ansatz $\widehat{u}_\mu = Z\widehat{\alpha}_\mu$ with $\widehat{u}_\mu = \widetilde{u}_\mu \circ \Phi_\mu^{-1}$, where $\widetilde{u}_\mu = Z\widehat{\alpha}_\mu, \;\; \Phi_\mu = \mathtt{N}(\widehat{a}_\mu)$.

- The composition with Φ_μ^{-1} corresponds to a mesh deformation.

  $\Rightarrow$ *easy to implement for SE/FE/FV discretizations*
- The action Φ_μ^{-1} should track sharp features of the solution field.

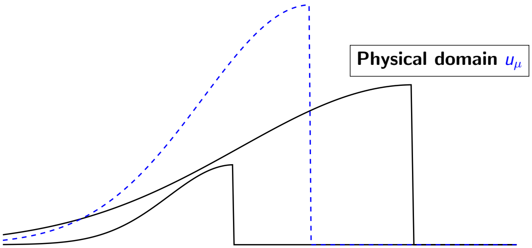

Nonlinear approximations (II): methods based on coordinate transformation

Intuition: in several cases, coherent structures (e.g., shocks) vary smoothly wrt μ.

Lagrangian ansatz: replace the linear ansatz $\widehat{u}_\mu = Z\widehat{\alpha}_\mu$ with $\widehat{u}_\mu = \widetilde{u}_\mu \circ \Phi_\mu^{-1}$, where $\widetilde{u}_\mu = Z\widehat{\alpha}_\mu, \;\; \Phi_\mu = \mathtt{N}(\widehat{a}_\mu)$.

- The composition with Φ_μ^{-1} corresponds to a mesh deformation.
  $\Rightarrow$ *easy to implement for SE/FE/FV discretizations*
- The action Φ_μ^{-1} should track sharp features of the solution field.

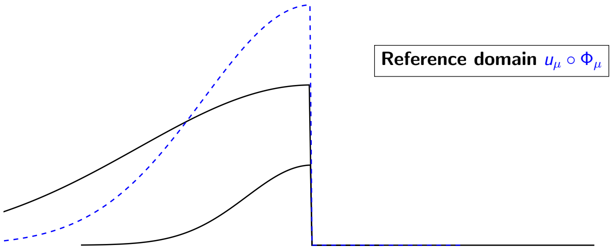

Registration task: find a parametric transformation that improves the compressibility of the solution set $\mathcal{M}$.

Aim of the talk: discuss recent advances on the development of registration methods for parametric model order reduction, with emphasis on advection-dominated flows.

1. Registration methods in bounded domains.
2. Registration-based model reduction.
3. Numerical results.

Registration methods in bounded domains

Parametric registration: given the snapshots $\mathcal{S}_{\rm train} := \{u^i = u_{\mu^i}\}_{i=1}^{n_{\rm train}} \subset \mathcal{M}$, we seek a parametric low-rank diffeomorphism $\mu \in \mathcal{P} \mapsto \Phi_\mu = \mathtt{N}(\widehat{a}_\mu)$.

For each parameter $\mu \in \mathcal{P}_{\rm train}$, we seek to minimize $\min_{\Phi \in \mathrm{Diff}_0(\overline{\Omega})} \mathfrak{f}^{\rm tg}(\Phi; \mu)$.

$\mathrm{Diff}_0(\overline{\Omega})$ is the set of diffeomorphisms that are isotopic to the identity.

intuition: we seek large yet continuous perturbations of the identity.

Challenges

- Choice of the target function (*what should we align?*)
- Choice of the parameterization $\mathtt{N}$ and dimensionality reduction.
- Generalization to unseen configurations. not covered in this talk

Data-rich scenario: ($\gtrsim \mathcal{O}(10^2)$)

$$\mathfrak{f}_\mu^{\rm tg}(\Phi) = \min_{\zeta \in \mathcal{Z}_n} \frac{1}{2} \int_\Omega (u_\mu \circ \Phi(\xi) - \zeta(\xi))^2 \, d\xi.$$

The space $\mathcal{Z}_n$ encodes our knowledge of the target and is built through a greedy procedure. TT, Zhang, M2AN, 2021.

Pros: well-aligned with the ultimate goal of registration (*compression of solution set*);

Cons: undesirable local minima for coarse (in space and parameter) discretizations.

Data-rich scenario: ($\gtrsim \mathcal{O}(10^2)$) $\qquad \mathfrak{f}_{\mu}^{\mathrm{tg}}(\Phi) = \min_{\zeta \in \mathcal{Z}_n} \frac{1}{2} \int_{\Omega} (u_\mu \circ \Phi(\xi) - \zeta(\xi))^2 \, d\xi.$

The space $\mathcal{Z}_n$ encodes our knowledge of the target and is built through a greedy procedure. TT, Zhang, M2AN, 2021.

Pros: well-aligned with the ultimate goal of registration (*compression of solution set*);

Cons: undesirable local minima for coarse (in space and parameter) discretizations.

Data-scarce scenario: ($\simeq \mathcal{O}(1)$) $\qquad \mathfrak{f}_{(2)}^{\mathrm{tg}}(\Phi) = \frac{1}{2} \sum_{i=1}^{N_0} \sum_{j=1}^{N_\mu} P_{i,j} \left\| \Phi(\xi_i) - y_j(\mu) \right\|_2^2;$

The points $\{\xi_i\}_{i=1}^{N}$ and $\{y_j(\mu)\}_{i=1}^{N_\mu}$ are extracted from the solution using an appropriate sensor (e.g., Ducros sensor for shocks). Labatut, Iollo, TT, Chapelier, CMAME, 2026.

Weights $P_{i,j}$ are computed using *expectation-maximization* Myronenko, Song, IEEE, 2010.

Pros: robust for very small (even $n_{\mathrm{train}} = 2$) datasets.

Cons: strong dependence on the choice of the sensor.

Major challenge: $\mathrm{Diff}_0(\overline{\Omega})$ is ∞-dimensional, non-convex set in $C^1(\overline{\Omega})$; bijectivity is not stable under small (in $C^1(\overline{\Omega})$) perturbations.

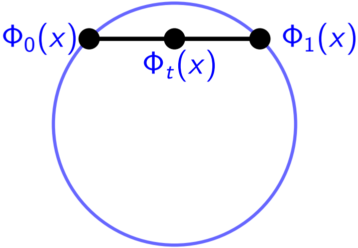

Example:

Φ_0, Φ_1 bijective in Ω

$\Phi_0(x) \neq \Phi_1(x)$ for some $x \in \partial\Omega$

$\Phi_t(x) = (1-t)\Phi_0(x) + t\Phi_1(x)$

is not a bijection in Ω for any $t \in (0,1)$.

Conclusion: traditional (affine) parameterizations $\mathtt{N}(x; a) = x + \sum_{i=1}^{M} a_i \varphi_i(x)$ are ill-suited for general domains.

Idea: we parameterize a pseudo-velocity v and set Φ as the flow of v, $\Phi = F[v]$.

$$\mathtt{N}(\xi, a) = X(\xi, t = 1, a), \quad \text{with} \quad \begin{cases} \dfrac{\partial X}{\partial t}(\xi, t, a) = v\left(X(\xi, t, a), t;\ a\right) & t \in (0, 1) \\ X(\xi, t = 0, a) = \xi \end{cases}$$

with $v\left(\xi, t;\ a\right) = \sum_{i=1}^{M} (a)_i \phi_i(\xi, t)$ and $\phi_i(\cdot, t) \cdot \mathbf{n}\big|_{\partial\Omega} \equiv 0$.

Idea: we parameterize a pseudo-velocity v and set Φ as the flow of v, $\Phi = F[v]$.

$$\mathtt{N}(\xi, a) = X(\xi, t=1, a), \quad \text{with} \begin{cases} \dfrac{\partial X}{\partial t}(\xi, t, a) = v\left(X(\xi, t, a), t;\, a\right) & t \in (0,1) \\ X(\xi, t=0, a) = \xi \end{cases}$$

with $v\left(\xi, t;\, a\right) = \sum_{i=1}^{M} (a)_i \phi_i(\xi, t)$ and $\phi_i(\cdot, t) \cdot \mathbf{n}\big|_{\partial\Omega} \equiv 0$.

Prior work: optimal transport (*Benamou&Brenier, 2000.,...*); image processing (*Beg et al, 2005; Younes 2010,...*); mesh morphing (*De Buhan et al, 2016; Kabalan et al, 2025*).

Novelty of our work: emphasis on bounded domains. Labatut et al, CMAME, 2026

Mathematical properties:

- $\Phi \in \mathrm{Diff}_0(\overline{\Omega})$ *if and only if* there exists $v \in C^1$ with $v(\cdot, t) \cdot \mathbf{n}\big|_{\partial\Omega} \equiv 0$ s.t. $\Phi = F[v]$.
- $\dfrac{\partial \mathtt{N}}{\partial a_i} = \nabla X(\xi, 1) \displaystyle\int_0^1 \left(\nabla X(\xi, \tau)\right)^{-1} \phi_i\left(X(\xi, \tau), \tau\right) d\tau, \quad \text{for} \;\; i = 1, \ldots, M.$

Observations: (i) the issue is the treatment of curved boundaries, (ii) bijectivity is preserved under composition.

Strategy (I): for polytopal domains, we directly parameterize the displacement $N(\cdot; a) = \mathtt{id} + \sum_{i=1}^{M} (a)_i \varphi_i$ with $\varphi_i \cdot \mathbf{n}\big|_{\partial\Omega} = 0$, $i = 1, \ldots, M$.

Strategy (II): for curved domains, we consider $N(a) = \Psi \circ \mathrm{N}_{\mathrm{p}}(a) \circ \Psi^{-1}$ with $N_{\mathrm{p}}(\cdot; a) = \mathtt{id} + \sum_{i=1}^{M} (a)_i \varphi_i$ and $\Psi : \Omega_{\mathrm{p}} \to \Omega$ and Ω_{p} is a polytope.

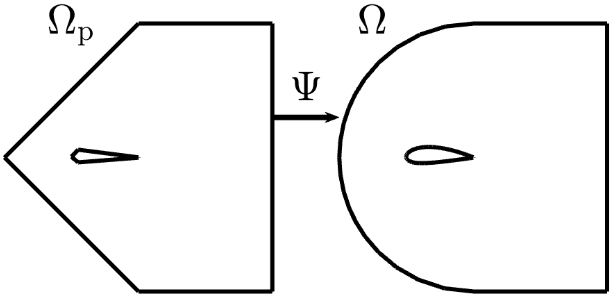

Parameterization of diffeomorphisms (III): compositional maps

Observations: (i) the issue is the treatment of curved boundaries, (ii) bijectivity is preserved under composition.

Strategy (I): for polytopal domains, we directly parameterize the displacement $N(\cdot; a) = \mathtt{id} + \sum_{i=1}^{M} (a)_i \varphi_i$ with $\varphi_i \cdot \mathbf{n}\big|_{\partial\Omega} = 0$, $i = 1, \ldots, M$.

Strategy (II): for curved domains, we consider $N(a) = \Psi \circ \mathrm{N}_{\rm p}(a) \circ \Psi^{-1}$ with $N_{\rm p}(\cdot; a) = \mathtt{id} + \sum_{i=1}^{M} (a)_i \varphi_i$ and $\Psi : \Omega_{\rm p} \to \Omega$ and $\Omega_{\rm p}$ is a polytope.

- The construction of Ψ exploits tools in high-order mesh generation.

- The method was proposed in [TT, 2020] and ameliorated/employed in subsequent works. [TT,Zhang, 2021], [Razavi,Yano,2025], [Reyes,Zahr,2025], [TT,2025]

Mathematical properties:

- If Ω is a polytope, $\Phi \in \mathrm{Diff}_0(\overline{\Omega})$ *if and only if* there exists $\varphi \in C^1$, $\varphi \cdot \mathbf{n}\big|_{\partial\Omega} = 0$ s.t. $\Phi = \mathtt{id} + \varphi$ and $J > 0$. *For curved domains, no universal approximation.*

Comments

Memo: CMs=compositional maps, VFs=vector flows.

- Evaluation of VFs involves the solution to an ODE for each $x \in \Omega$, while CMs can be directly evaluated. Evaluation of VFs is slower.
- Bijectivity of VFs is guaranteed for *exact* time integration.
  Bijectivity requires accurate integration in the proximity of the boundary.

- If regression is employed, it is difficult to ensure bijectivity of CMs for out-of-sample parameters.

- Expressivity of CMs for curved domains depends on the choice of Ψ.

Comments

Memo: CMs=compositional maps, VFs=vector flows.

- Evaluation of VFs involves the solution to an ODE for each $x \in \Omega$, while CMs can be directly evaluated. Evaluation of VFs is slower.
- Bijectivity of VFs is guaranteed for *exact* time integration. Bijectivity requires accurate integration in the proximity of the boundary.

- If regression is employed, it is difficult to ensure bijectivity of CMs for out-of-sample parameters.

- Expressivity of CMs for curved domains depends on the choice of Ψ.

Conclusion: both approaches have strengths and limitations.

- **Challenge of VFs:** rapid time integration schemes.

- **Challenge of CMs:** automated construction of Ψ and Ω_{p} (for curved domains).

Registration-based model reduction

- Projection-based model reduction
- Nonlinear interpolation

Toward the application to model reduction (I)

Parametric registration: given the snapshots $S_{\rm train} := \{u^i = u_{\mu^i}\}_{i=1}^{n_{\rm train}} \subset \mathcal{M}$, we seek a parametric low-rank diffeomorphism $\mu \in \mathcal{P} \mapsto \Phi_\mu = \mathtt{N}(\widehat{a}_\mu)$.

Question: how can we employ registration in MOR?

Toward the application to model reduction (I)

Parametric registration: given the snapshots $S_{\rm train} := \{u^i = u_{\mu^i}\}_{i=1}^{n_{\rm train}} \subset \mathcal{M}$, we seek a parametric low-rank diffeomorphism $\mu \in \mathcal{P} \mapsto \Phi_\mu = \mathtt{N}(\widehat{a}_\mu)$.

Question: how can we employ registration in MOR?

- **Interpolation:** exploit coordinate transformations to perform nonlinear interpolation of solution fields.
- **Data augmentation:** exploit coordinate transformations to generate synthetic snapshots $\notin \mathrm{span}(S_{\rm train})$ for POD-based MOR. *generative modeling*
- **Projection-based MOR**: exploit residual minimization for prediction. PMOR methods rely on the *Lagrangian ansatz:* $\widehat{u}_\mu = \widetilde{u}_\mu \circ \Phi_\mu^{-1}$ with $\widetilde{u}_\mu = Z\widehat{\alpha}_\mu, \;\; \Phi_\mu = \mathtt{N}(\widehat{a}_\mu)$.

  Approach 1: only $\widehat{\alpha}_\mu$ is computed through residual minimization;

  Approach 2: both $\widehat{\alpha}_\mu$ and $\widehat{a}_\mu$ are computed through residual minimization.

Toward the application to model reduction (II): comments

Nonlinear interpolation:

Mojgani&Balajewicz, Proc. AIAA, 2021; Sarna&Benner, CMAME, 2021; Iollo&Taddei, JCP 2022; Van Heyningen et al.. Int J Comput Fluid D, 2023.

Data augmentation:

Bernard, Iollo, Riffaud, JCP 2018; Cucchiara et al. JCP, 2024.

Projection-based MOR:

Approach 1: Cagniart et al, 2019; Taddei, SISC 2020; Ching et al., AIAA, 2022; Razavi&Yano, JCP, 2025...

Approach 2: Mirhoseini&Zahr, JCP, 2023.

Toward the application to model reduction (II): comments

Nonlinear interpolation:

Mojgani&Balajewicz, Proc. AIAA, 2021; Sarna&Benner, CMAME, 2021; Iollo&Taddei, JCP 2022; Van Heyningen et al.. Int J Comput Fluid D, 2023.

Data augmentation:

Bernard, Iollo, Riffaud, JCP 2018; Cucchiara et al. JCP, 2024.

Projection-based MOR:

Approach 1: Cagniart et al, 2019; Taddei, SISC 2020; Ching et al., AIAA, 2022; Razavi&Yano, JCP, 2025...

Approach 2: Mirhoseini&Zahr, JCP, 2023.

Given Φ, the first PMOR approach exploits well-established tools in linear RBM in parametric geometries.

- Projection-based model reduction
- Nonlinear interpolation

Projection-based model reduction with mesh adaptation: [Barral,TT,Tifouti, JCP,2024]

Initialization: $\Phi^{(0)} = \texttt{id}$, $\mathcal{P}_{\rm train} \subset \mathcal{P}$, $\mathcal{T}_{\rm hf}^{(0)} = \mathcal{T}_{\rm hf}^{(1)}$, $\left(Z^{(0)}, \mathrm{ROM}^{(0)}\right)$.

`For` $k = 1, \ldots, N_{\rm it}$

1. Snapshot generation $\left(Z^{(k-1)}, \mathrm{ROM}^{(k-1)}\right) \Rightarrow \mathcal{S}^{(k-1)} = \{u_\mu^{\rm hf,(k-1)} : \mu \in \mathcal{P}_{\rm train}\}$
2. `if` $k > 1$, Parametric mesh adaptation $\mathcal{S}^{(k-1)} \Rightarrow \mathcal{T}_{\rm hf}^{(k)}$
3. Registration $\left(\mathcal{S}^{(k-1)}, \mathcal{T}_{\rm hf}^{(k)}\right) \Rightarrow \Phi^{(k)}$
4. MOR training $\left(\Phi^{(k)}, \mathcal{T}_{\rm hf}^{(k)}\right) \Rightarrow \left(Z^{(k)}, \mathrm{ROM}^{(k)}\right)$

`EndFor`

Projection-based model reduction with mesh adaptation: [Barral,TT,Tifouti, JCP,2024]

Initialization: $\Phi^{(0)} = \mathtt{id}$, $\mathcal{P}_{\rm train} \subset \mathcal{P}$, $\mathcal{T}_{\rm hf}^{(0)} = \mathcal{T}_{\rm hf}^{(1)}$, $\left(Z^{(0)}, \mathrm{ROM}^{(0)}\right)$.

For $k = 1, \ldots, N_{\rm it}$

1. Snapshot generation $\left(Z^{(k-1)}, \mathrm{ROM}^{(k-1)}\right) \Rightarrow \mathcal{S}^{(k-1)} = \{u_\mu^{\rm hf,(k-1)} : \mu \in \mathcal{P}_{\rm train}\}$
2. if $k > 1$, Parametric mesh adaptation $\mathcal{S}^{(k-1)} \Rightarrow \mathcal{T}_{\rm hf}^{(k)}$
3. Registration $\left(\mathcal{S}^{(k-1)}, \mathcal{T}_{\rm hf}^{(k)}\right) \Rightarrow \Phi^{(k)}$
4. MOR training $\left(\Phi^{(k)}, \mathcal{T}_{\rm hf}^{(k)}\right) \Rightarrow \left(Z^{(k)}, \mathrm{ROM}^{(k)}\right)$

EndFor

- The for loop addresses inaccuracy of early-stage HF simulations;
- MOR training can be performed using standard linear MOR methods for parametric geometries;
- We re-use information from previous iterations needs to speed up the training phase.

not covered in this talk.

1. Piecewise approximations. We include a clustering step in parameter space to handle *shock-topology changes*.

Keywords: k-SVD/k-medoids clustering; LSPG model reduction.

2. Goal-oriented approximations. We include a ROM for adjoint to effectively estimate quantities of interest.

ROM estimate: $\widehat{J}(\widehat{u}_\mu, \widehat{\psi}_\mu; \mu) = J_{\text{target}}(\widehat{u}_\mu; \mu) - \mathfrak{R}\left(\widehat{u}_\mu, \widehat{\psi}_\mu; \mu\right).$

Keywords: dual-weighted residual error estimation; hierarchical error estimation.

N Barral, TT, I Tifouti, *Local registration-based model reduction of parameterized PDEs with spatio-parameter adaptivity*, AIAA SciTech 2025.
N Barral, TT, I Tifouti, *Goal-oriented registration-based model reduction of shock-dominated flows with spatio-parameter adaptivity, in preparation.*

Extensions (PhD thesis of I Tifouti)

1. Piecewise approximations. We include a clustering step in parameter space to handle *shock-topology changes*.

Keywords: k-SVD/k-medoids clustering; LSPG model reduction.

2. Goal-oriented approximations. We include a ROM for adjoint to effectively estimate quantities of interest.

ROM estimate: $\widehat{J}(\widehat{u}_\mu, \widehat{\psi}_\mu; \mu) = J_{\text{target}}(\widehat{u}_\mu; \mu) - \mathfrak{R}\left(\widehat{u}_\mu, \widehat{\psi}_\mu; \mu\right).$

Keywords: dual-weighted residual error estimation; hierarchical error estimation.

The registration algorithm is a tool that can be integrated in various MOR workflows, to address a broad range of computational mechanics tasks.

N Barral, TT, I Tifouti, *Local registration-based model reduction of parameterized PDEs with spatio-parameter adaptivity*, AIAA SciTech 2025.

N Barral, TT, I Tifouti, *Goal-oriented registration-based model reduction of shock-dominated flows with spatio-parameter adaptivity, in preparation*.

Registration-based model reduction

- Projection-based model reduction
- Nonlinear interpolation

Nonlinear interpolation via convex displacement interpolation [Iollo, TT, JCP, 2022]

Task: determine a nonlinear interpolation $\widehat{u}:\Omega\times[0,1]\to\mathbb{R}^D$ between the snapshots $u_0 := u_{\mu^0}$ and $u_1 := u_{\mu^1}$.

Strategy: given $s\in[0,1]$,

1. apply registration to determine the mapping $\Phi = F[v]$;
2. define $\Phi_{s\to 0}(\xi) = Y(\xi, t=0)$ and $\Phi_{s\to 1}(\xi) = X(\xi, t=1)$ where X and Y are the forward and the backward flows associated with the velocity v,

$$\begin{cases} \frac{\partial X}{\partial t}(\xi,t) = v(X(\xi,t),t) & t\in(s,1], \\ X(\xi,s)=\xi, \end{cases} \qquad \begin{cases} \frac{\partial Y}{\partial t}(\xi,t) = -v(Y(\xi,t),t) & t\in[0,s), \\ Y(\xi,s)=\xi, \end{cases}$$

3. return the estimate $\widehat{u}(\xi,s) = (1-s)u_0\circ\Phi_{s\to 0}(\xi) + s u_1\circ\Phi_{s\to 1}(\xi) \quad \xi\in\Omega.$

Nonlinear interpolation via convex displacement interpolation [Iollo, TT, JCP, 2022]

Task: determine a nonlinear interpolation $\widehat{u} : \Omega \times [0,1] \to \mathbb{R}^D$ between the snapshots $u_0 := u_{\mu^0}$ and $u_1 := u_{\mu^1}$.

Strategy: given $s \in [0,1]$,

1. apply registration to determine the mapping $\Phi = F[v]$;
2. define $\Phi_{s\to 0}(\xi) = Y(\xi, t=0)$ and $\Phi_{s\to 1}(\xi) = X(\xi, t=1)$ where X and Y are the forward and the backward flows associated with the velocity v,

$$\begin{cases} \frac{\partial X}{\partial t}(\xi,t) = v(X(\xi,t),t) & t \in (s,1], \\ X(\xi,s) = \xi, \end{cases} \qquad \begin{cases} \frac{\partial Y}{\partial t}(\xi,t) = -v(Y(\xi,t),t) & t \in [0,s), \\ Y(\xi,s) = \xi, \end{cases}$$

3. return the estimate $\widehat{u}(\xi,s) = (1-s)u_0 \circ \Phi_{s\to 0}(\xi) + s u_1 \circ \Phi_{s\to 1}(\xi) \quad \xi \in \Omega$.

• CDI can be combined with compositional maps and can be extended to multiple parameters. Cucchiara et al, JCP, 2024.

Interpretation: CDI corresponds to a convex interpolation along characteristics of the vector field v.

$$\widehat{u}(x,s) = (1-s)u_0 \circ \Phi_{s\to 0}(x) + s u_1 \circ \Phi_{s\to 1}(x) \quad \xi \in \Omega.$$

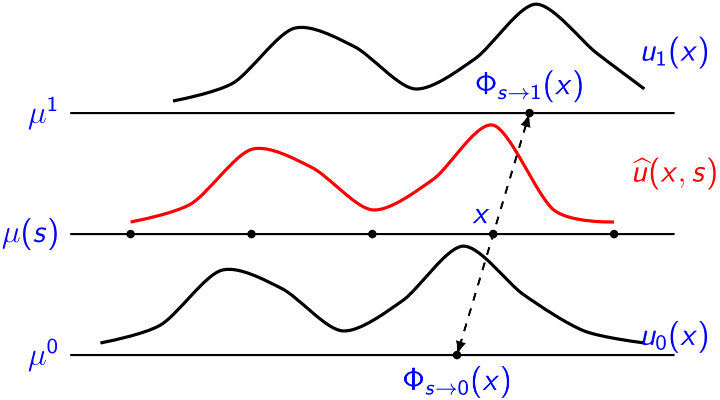

Interpretation: CDI corresponds to a convex interpolation along characteristics of the vector field v.

$$\widehat{u}(x,s) = (1-s)u_0 \circ \Phi_{s\to 0}(x) + s u_1 \circ \Phi_{s\to 1}(x) \quad \xi \in \Omega.$$

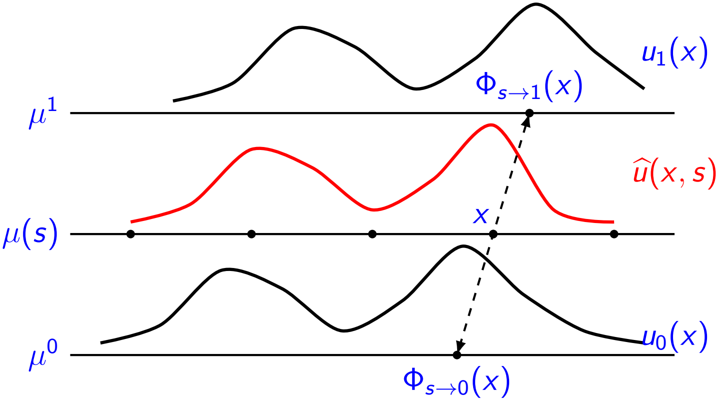

Note that $\widehat{u}(\cdot,s) \notin \mathrm{span}\{u_0, u_1\} \Rightarrow$ CDI is useful for **data augmentation**.

Numerical results

- Inviscid flow past an array of LS89 blades
- Turbulent flow over an ONERA M6 wing (Jon Labatut)

Numerical results

- Inviscid flow past an array of LS89 blades
- Turbulent flow over an ONERA M6 wing (Jon Labatut)

Steady-state compressible Euler equations for ideal gases ($\gamma = 1.4$).

Challenges: periodic BCs; several coherent structures (shock, wakes), geometry parameterization.

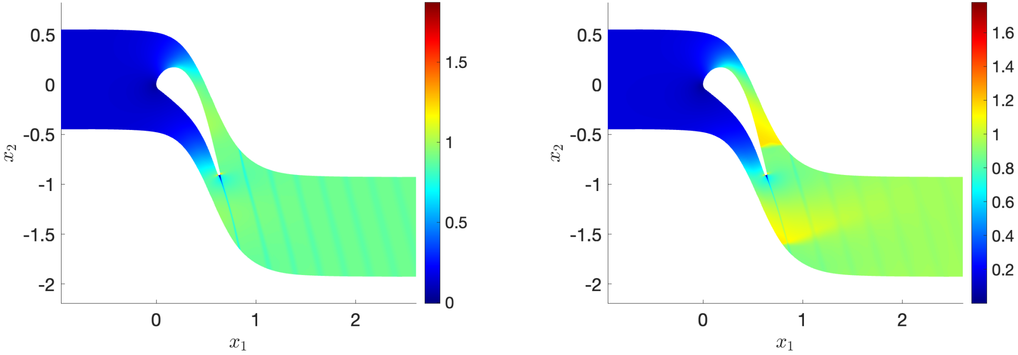

Steady-state compressible Euler equations for ideal gases ($\gamma = 1.4$).

Challenges: periodic BCs; several coherent structures (shock, wakes), geometry parameterization.

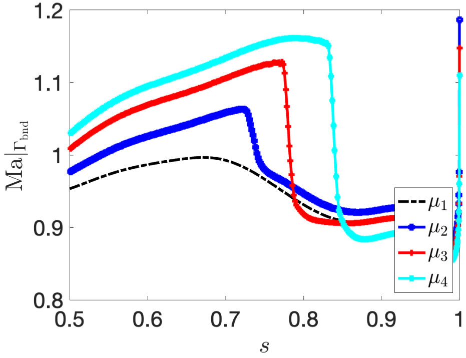

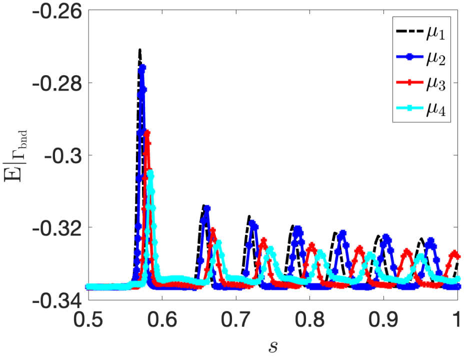

We perform $N_{\mathrm{it}} = 3$ iterations of the adaptive procedure.

- We consider a P2 DG discretization with dilation-based AV.
  Yu, Hesthaven, CiCP, 2020.
- Snapshot generation is performed using the available ROM from the previous iteration.
- We validate performance over $n_{\mathrm{test}} = 20$ out-of-sample parameters.

We perform $N_{\text{it}} = 3$ iterations of the adaptive procedure.

- We consider a P2 DG discretization with dilation-based AV.
  Yu, Hesthaven, CiCP, 2020.
- Snapshot generation is performed using the available ROM from the previous iteration.
- We validate performance over $n_{\text{test}} = 20$ out-of-sample parameters.

Metrics

L^2 relative error: $E_\mu^{\text{hf}} = \dfrac{\| u_\mu^{\text{hf}} - \widehat{u}_\mu \|_{L^2(\Omega)}}{\| u_\mu^{\text{hf}} \|_{L^2(\Omega)}}$;

L^2 sub-optimality index: $\eta_\mu^{\text{hf}} = \dfrac{\| u_\mu^{\text{hf}} - \widehat{u}_\mu \|_{L^2(\Omega)}}{\min_{\zeta \in \mathcal{Z}_n} \| u_\mu^{\text{hf}} - \zeta \|_{L^2(\Omega)}}$;

error in total enthalpy: $E_\mu^{\infty} = \dfrac{\| H_\mu^{\text{hf}} - H_\mu^{\text{th}} \|_{L^2(\Omega)}}{\| H_\mu^{\text{th}} \|_{L^2(\Omega)}}$. HF error indicator.

Results (I): model reduction

We rely on

- LSPG projection with element/edge-wise EQ hyper-reduction;
- discretize-then-map (DtM) approach to handle geometry variations;
- greedy sampling driven by residual indicator $n(it) = [15, 17, 25]$.

Greedy sampling terminates when the relative error associated with the new snapshot is less than 0.1%.

Right: relative L^2 error.

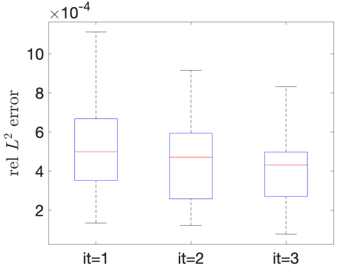

References: MoRePaS community (now MORE...).

Results (I): model reduction

We rely on

- LSPG projection with element/edge-wise EQ hyper-reduction;
- discretize-then-map (DtM) approach to handle geometry variations;
- greedy sampling driven by residual indicator $n(it) = [15, 17, 25]$.

Greedy sampling terminates when the relative error associated with the new snapshot is less than 0.1%.

Right: sub-optimality index.

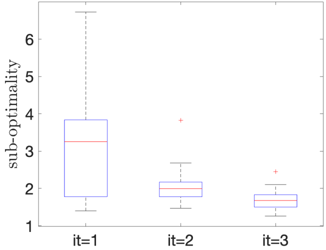

References: MoRePaS community (now MORE...).

Results (I): model reduction

We rely on

- LSPG projection with element/edge-wise EQ hyper-reduction;
- discretize-then-map (DtM) approach to handle geometry variations;
- greedy sampling driven by residual indicator $n(it) = [15, 17, 25]$.

Greedy sampling terminates when the relative error associated with the new snapshot is less than 0.1%.

Right: enthalpy error.

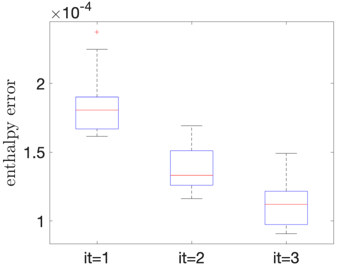

References: MoRePaS community (now MORE...).

Results (I): model reduction

We rely on

- LSPG projection with element/edge-wise EQ hyper-reduction;
- discretize-then-map (DtM) approach to handle geometry variations;
- greedy sampling driven by residual indicator $n(it) = [15, 17, 25]$.

Greedy sampling terminates when the relative error associated with the new snapshot is less than 0.1%.

Right: wall-clock online cost.

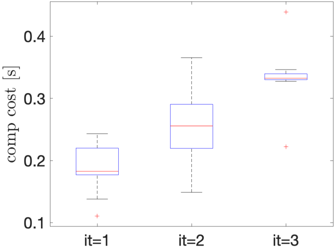

References: MoRePaS community (now MORE...).

We consider CMs; the objective combines distributed and point-set sensors.

Figure (left): Mach number on the upper side of the blade.

Figure (right): Entropy on the lower boundary.

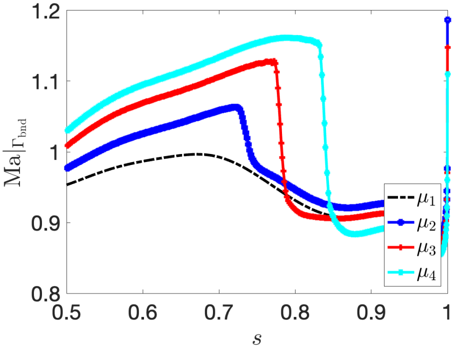

(a) phys config.

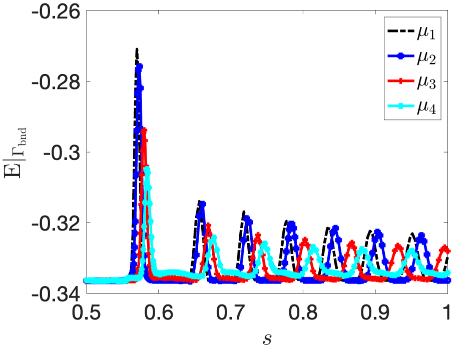

(b) phys config.

We consider CMs; the objective combines distributed and point-set sensors.

Figure (left): Mach number on the upper side of the blade.

Figure (right): Entropy on the lower boundary.

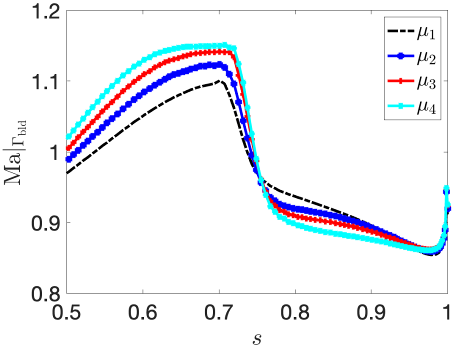

(a) reference config.

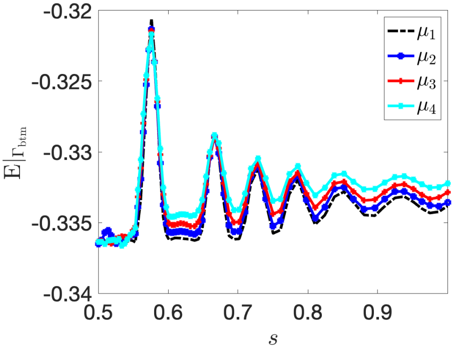

(b) reference config.

Results (II): registration (iteration 2)

We consider CMs; the objective combines distributed and point-set sensors.

Figure (left): Mach number on the upper side of the blade.

Figure (right): Entropy on the lower boundary.

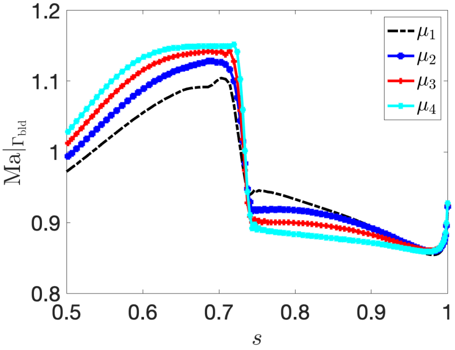

(a) reference config.

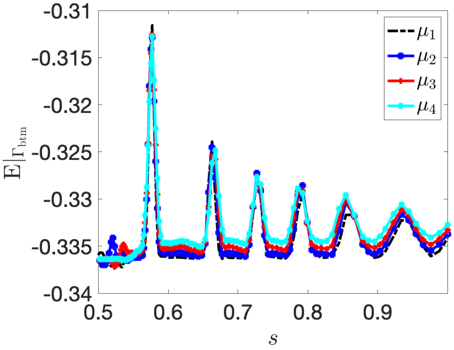

(b) reference config.

We consider CMs; the objective combines distributed and point-set sensors.

Figure (left): Mach number on the upper side of the blade.

Figure (right): Entropy on the lower boundary.

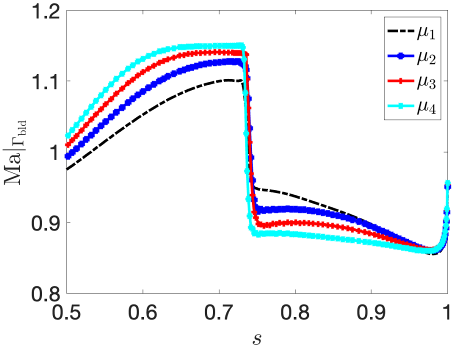

(a) reference config.

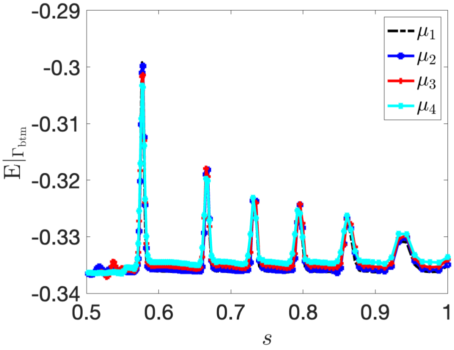

(b) reference config.

Results (III): mesh adaptation (iteration 1)

We rely on a mark-then-refine strategy driven by the local variation of total enthalpy and the norm of the gradient of the entropy.

Implementation is based on the Inria software MMG.

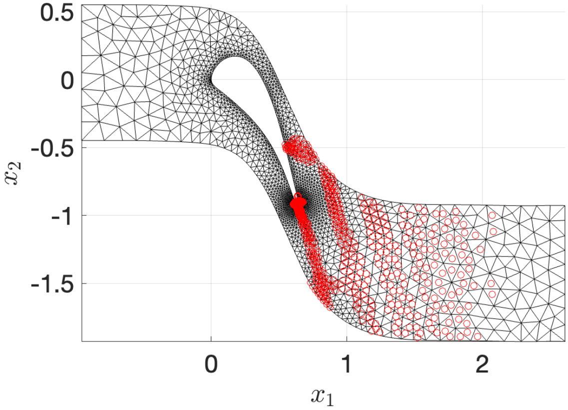

Results (III): mesh adaptation (iteration 2)

We rely on a mark-then-refine strategy driven by the local variation of total enthalpy and the norm of the gradient of the entropy.

Implementation is based on the Inria software MMG.

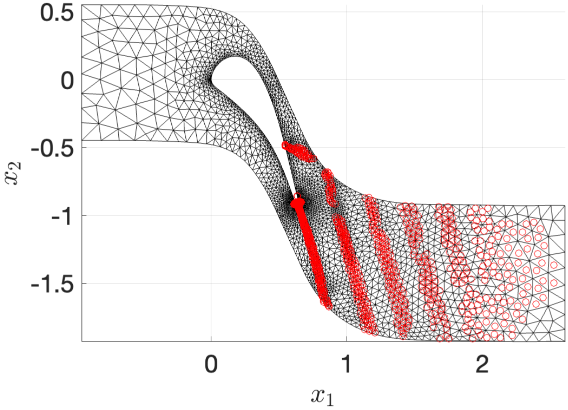

Results (III): mesh adaptation (iteration 3)

We rely on a mark-then-refine strategy driven by the local variation of total enthalpy and the norm of the gradient of the entropy.

Implementation is based on the Inria software MMG.

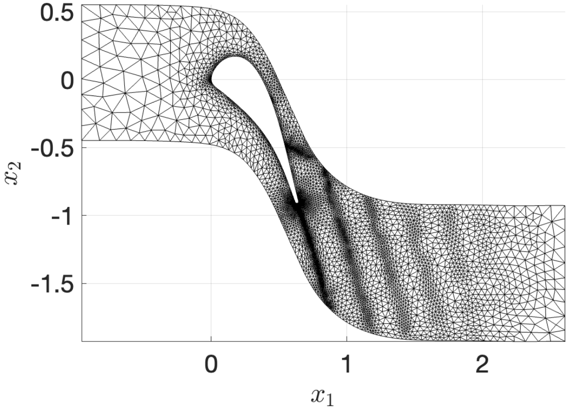

Results (III): mesh adaptation (iteration 3)

We rely on a mark-then-refine strategy driven by the local variation of total enthalpy and the norm of the gradient of the entropy.

Implementation is based on the Inria software MMG.

Interpretation: we rely on two separate mesh adaptation mechanisms:

- parameter-independent *h*-refinement;
- parameter-dependent *r*-refinement based on registration.

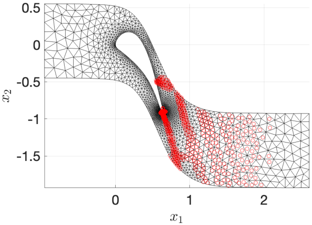

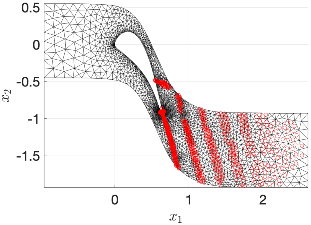

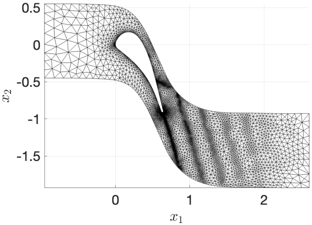

Results (IV): offline computational costs (total 5h 33')

Percentage of offline costs of the last greedy algorithm : $\approx 72\%$.
$\Rightarrow$ offline costs comparable with state-of-the-art linear method.

	it = 1	it = 2	it = 3
ROB size:	15	17	25
mesh elements:	4249	7398	13396
snapshot generation:	1213.35	12.07	14.82
registration (sensor def.):	139.00	153.25	167.22
registration (optimization):	304.52	423.77	1147.62
mesh adaptation:	0.00	3.53	1.45
greedy alg (HF solves):	226.90	1457.03	12899.77
greedy alg (overhead):	87.65	313.90	1446.37
PTC iterations (avg):	6.40	18.18	51.88

Numerical results

- Inviscid flow past an array of LS89 blades
- Turbulent flow over an ONERA M6 wing (Jon Labatut)

Parameter: $\mathrm{AoA} \in [3.06^o, 5.1^o]$, $\mathrm{Re} = 14.6 \cdot 10^6$, $\mathrm{Ma}_\infty = 0.84$.

Fluid model: compressible RANS; turbulence model = Spalart Allmaras.

Numerical model: DG P1 (nbr elements $10.8 \cdot 10^6$)[1].

Flow densities for $\mathrm{AoA} = 3.06^o$ *and* $\mathrm{AoA} = 5.1^o$.

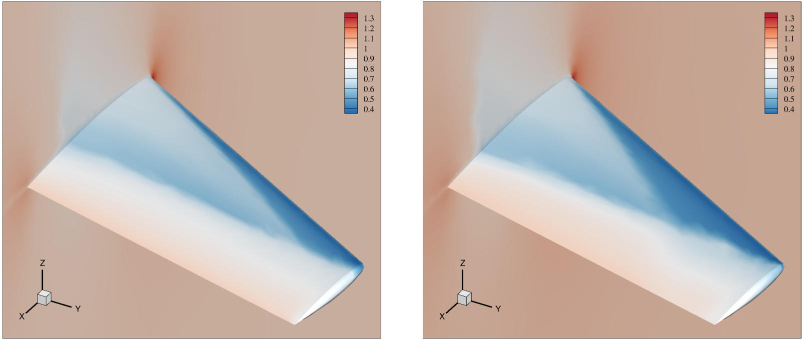

[1]Simulations are performed using the Onera-Airbus-DLR software `CODA`.

Application of CDI (I)

We consider vector flows. The target function exploits point-set sensor based on

$$s(x;\mu) = \frac{v_\mu(x) \cdot \nabla p_\mu(x)}{\|\nabla p_\mu(x)\|_2 a_{\infty,\mu}}$$

cf. TecPlot manual

Comparison of source and mapped source points with sensor activation surface.

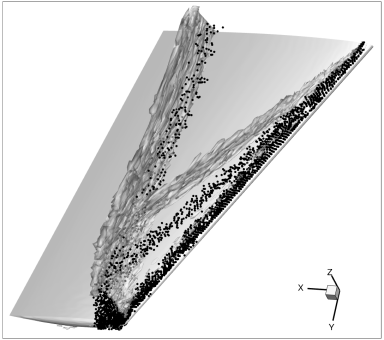

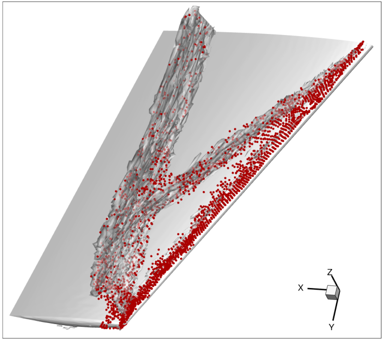

Application of CDI (I)

We consider vector flows. The target function exploits point-set sensor based on

$$s(x;\mu) = \frac{v_\mu(x) \cdot \nabla p_\mu(x)}{\|\nabla p_\mu(x)\|_2 a_{\infty,\mu}}$$

cf. TecPlot manual

CDI prediction of flow density ($s = 0$)

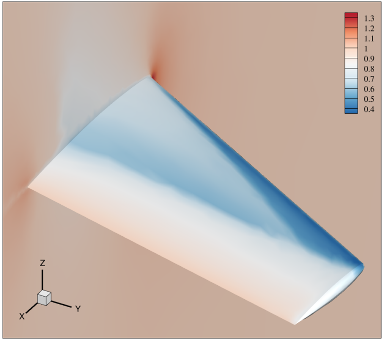

Application of CDI (I)

We consider vector flows. The target function exploits point-set sensor based on

$$s(x;\mu) = \frac{v_\mu(x) \cdot \nabla p_\mu(x)}{\|\nabla p_\mu(x)\|_2 a_{\infty,\mu}}$$

cf. TecPlot manual

CDI prediction of flow density ($s = 0.25$)

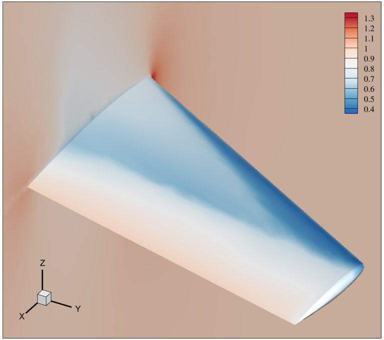

Application of CDI (I)

We consider vector flows. The target function exploits point-set sensor based on

$$s(x;\mu) = \frac{v_\mu(x) \cdot \nabla p_\mu(x)}{\|\nabla p_\mu(x)\|_2 a_{\infty,\mu}}$$ cf. TecPlot manual

CDI prediction of flow density ($s = 0.5$)

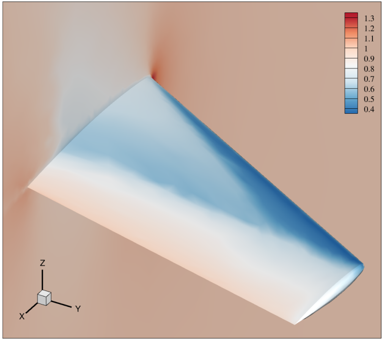

We consider vector flows. The target function exploits point-set sensor based on

$$s(x;\mu) = \frac{v_\mu(x)\cdot\nabla p_\mu(x)}{\|\nabla p_\mu(x)\|_2 a_{\infty,\mu}}$$

cf. TecPlot manual

CDI prediction of flow density ($s = 0.75$)

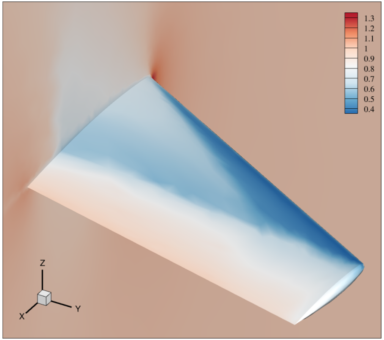

We consider vector flows. The target function exploits point-set sensor based on

$$s(x;\mu) = \frac{v_\mu(x)\cdot\nabla p_\mu(x)}{\|\nabla p_\mu(x)\|_2 a_{\infty,\mu}}$$

cf. TecPlot manual

CDI prediction of flow density ($s = 1$)

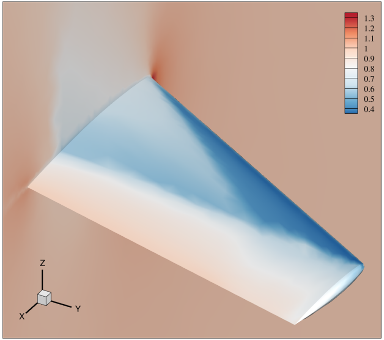

Idea: use CDI estimate as initial condition for the FOM.

Results: CDI estimate enables 3x reduction of the number of Newton's iterations to meet the convergence criterion.

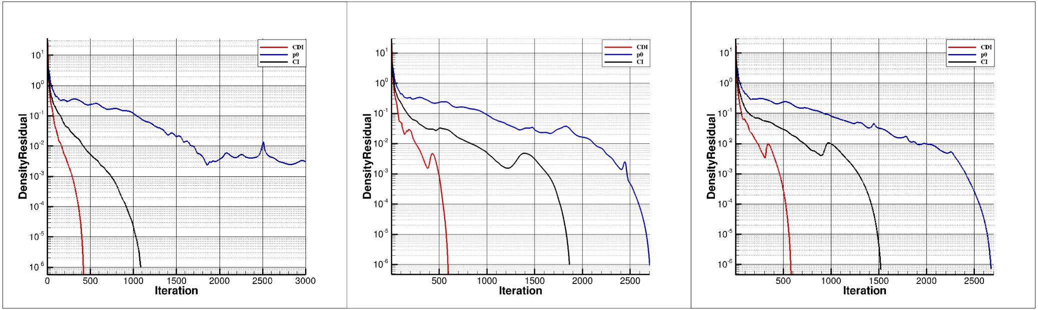

(a) $AoA = 3.57^o$ ($s = 0.25$) (b) $AoA = 4.08^o$ ($s = 0.5$) (c) $AoA = 4.59^o$ ($s = 0.75$)

Idea: use CDI estimate for data augmentation.

Results: We compare the projection error obtained using the dataset of two HF snapshots (red) and the augmented dataset with 500 artificial snapshots generated using CDI (blue).

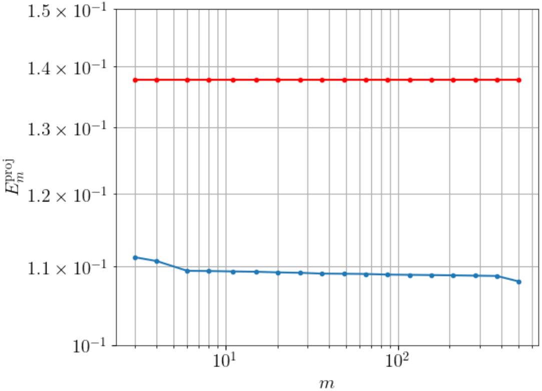

Conclusions

Summary and perspectives

Transport phenomena are challenging for MOR due to the inadequacy of linear approximations and the need for parameter-dependent adaptive meshes.

We proposed a framework based on **registration** that is tailored to parametric problems with smoothly-varying *coherent structures with compact support* (e.g., shocks, shear layers, cracks).

We prioritized **parsimonious offline training** through parameter-dependent mesh adaptation (via registration) and data augmentation (via nonlinear interpolation).

Focus on data-scarce scenarios

Summary and perspectives

Transport phenomena are challenging for MOR due to the inadequacy of linear approximations and the need for parameter-dependent adaptive meshes.

We proposed a framework based on **registration** that is tailored to parametric problems with smoothly-varying *coherent structures with compact support* (e.g., shocks, shear layers, cracks).

We prioritized **parsimonious offline training** through parameter-dependent mesh adaptation (via registration) and data augmentation (via nonlinear interpolation).

Focus on data-scarce scenarios

Connection with other nonlinear ansatzes: methods based on coordinate transformations fit in the growing literature on *nonlinear approximations*. Ultimately, the choice should be a compromise between expressivity and learnability.
$\Rightarrow$ Mathematical analysis is needed to understand strengths and limitations of the approach *for specific classes of engineering problems.*

Thank you for your attention!

For more information, please check:

- N Barral, TT, I Tifouti. *Registration-based model reduction of parameterized PDEs with spatio-parameter adaptivity*. JCP, 2024.
- TT. *Compositional maps for registration in complex geometries*. SISC, 2025.
- N Barral, TT, I Tifouti. *Local registration-based model reduction of parameterized PDEs With spatio-parameter adaptivity*. AIAA SciTech, 2025.
- J Labatut, A Iollo, TT, J-B Chapelier. *Parametric vector flows for registration fields in bounded domains with applications to nonlinear interpolation of shock-dominated flows.* CMAME, 2026.
- A Iollo, J Labatut, P Mounoud, TT. *Mathematical aspects of registration methods in bounded domains.* Arxiv, 2026.

Backup

- A bit of analysis
- Piecewise-Lagrangian approximations

Backup

- A bit of analysis
- Piecewise-Lagrangian approximations

A working example (Taddei, SISC, 2020)

Define $u : (0,1)^2 \times \mathcal{P} \to \{0,1\}$ s.t. $u_\mu(x) = \mathbb{1}_{f_\mu(x_1)<x_2}(x)$.

Assume $f_\mu([0,1]) \subset [\delta, 1-\delta]$ for all $\mu \in \mathcal{P}$. Define

$$\mathcal{C}_{n,m}^{\mathrm{lag}} = \Big\{ \mathtt{Z} : \mathtt{Z} = \mathtt{Z}^{\mathrm{lin}} \circ \boldsymbol{\Phi}^{-1}, \ \mathrm{s.t.} \quad \mathtt{Z}^{\mathrm{lin}}(\boldsymbol{\alpha}) = \sum_{i=1}^{n} (\boldsymbol{\alpha})_i \zeta_i, \quad \boldsymbol{\Phi}(\mathbf{a}) = \mathtt{id} + \sum_{i=1}^{m} (\mathbf{a})_i \varphi_i \Big\}$$

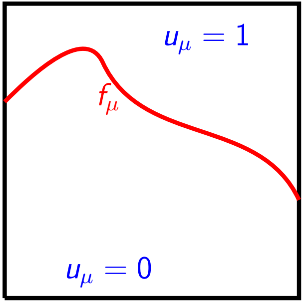

$$\Rightarrow \mathfrak{d}\left(\mathcal{M}, \mathcal{C}_{n,m}^{\mathrm{lag}}, \|\cdot\|_{L^1(\Omega)}\right) \leq C \, \frac{\mathfrak{d}\left(\mathcal{M}_{\mathrm{f}}, \mathcal{C}_{m}^{\mathrm{lin}}, \|\cdot\|_{\mathrm{Lip}([0,1])}\right)}{\sqrt{n}},$$

Multiplicative effect between n and m convergence.

Source: Ferrero, TT, Zhang, JCP, 2022.

Test case: inviscid supersonic flow past a parametric bump (no topology changes).

Remark: differences increase as we refine the mesh.

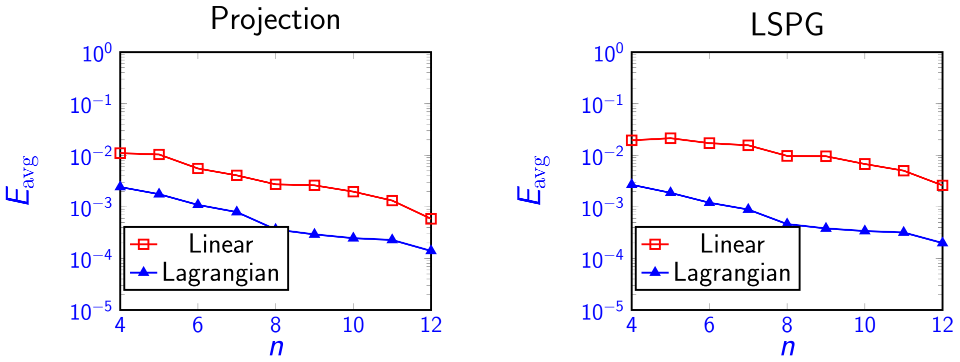

(a) (b)

Backup

- A bit of analysis
- Piecewise-Lagrangian approximations

Supersonic flow past a Gaussian bump (I)

Steady-state compressible Euler equations for ideal gases ($\gamma = 1.4$).

- Wall BCs at lower and upper boundaries; the full far-field state is prescribed at the inflow.

Parameterization: $\mu = [\mu_1, \mu_2] \in \mathcal{P}$

- bump $y_\mu(x_1) = \mu_1 e^{-25x_1^2}$, $\mu_1 \in [0.05, 0.065]$.
- free-stream Mach $\mathrm{Mach}_\infty = \mu_2 \in [1.6, 3]$.

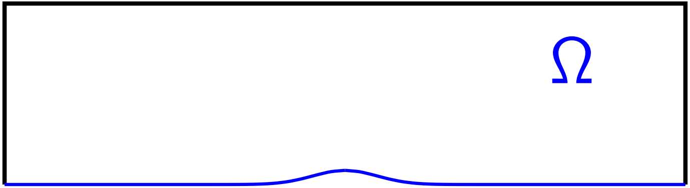

Supersonic flow past a Gaussian bump (II)

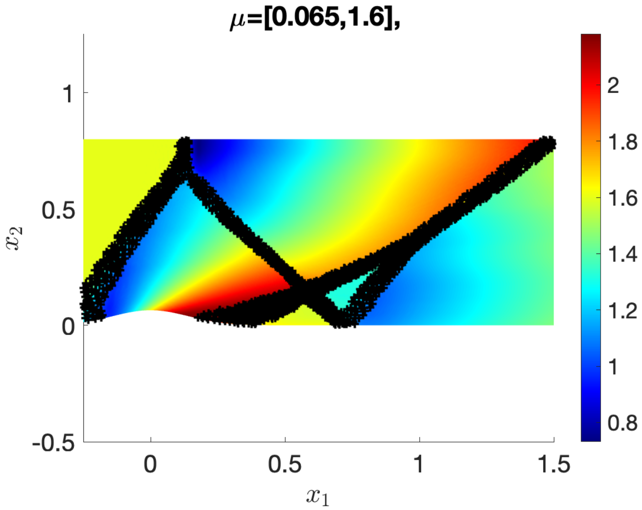

Iterative procedure (Lagrangian)

Initialization: $\Phi^{(0)} = \mathtt{id}$, $\mathcal{P}_{\rm train} \subset \mathcal{P}$, $\mathcal{T}_{\rm hf}^{(0)} = \mathcal{T}_{\rm hf}^{(1)}$.

`For` $k = 1, \ldots, N_{\rm it}$

1. Snapshot generation $\qquad \mathcal{T}_{\rm hf}^{(k-1)} \Rightarrow \mathcal{S}^{(k-1)} = \{u_{\mu}^{\rm hf,(k-1)} : \mu \in \mathcal{P}_{\rm train}\}$
2. `if` $k > 1$, Parametric mesh adaptation $\qquad \mathcal{S}^{(k-1)} \Rightarrow \mathcal{T}_{\rm hf}^{(k)}$
3. Registration $\qquad \left(\mathcal{S}^{(k-1)}, \mathcal{T}_{\rm hf}^{(k)}\right) \Rightarrow \Phi^{(k)}$
4. MOR training $\qquad \left(\Phi^{(k)}, \mathcal{T}_{\rm hf}^{(k)}\right) \Rightarrow \left(Z^{(k)}, {\rm ROM}^{(k)}\right)$

`EndFor`

New iterative procedure (piecewise Lagrangian)

Initialization: $\Phi^{(0)} = \mathtt{id}$, $\mathcal{P}_{\rm train} \subset \mathcal{P}$, $\mathcal{T}_{\rm hf}^{(0)} = \mathcal{T}_{\rm hf}^{(1)}$.

1. Snapshot generation $\quad \mathcal{T}_{\rm hf}^{(0)} \Rightarrow \mathcal{S}^{(0)} = \{u_\mu^{\rm hf,(0)} : \mu \in \mathcal{P}_{\rm train}\}$

2. Clustering: $\quad \mathcal{S}^{(0)} \Rightarrow \{\mathcal{P}_{\rm train}^{(1,i)}\}_{i=1}^{\kappa}$

`For` $k = 1, \ldots, N_{\rm it}$

`For` $i = 1, \ldots, \kappa$

i.3. Snapshot generation $\quad \mathcal{T}_{\rm hf}^{(k-1,i)} \Rightarrow \mathcal{S}^{(k-1,i)} = \{u_\mu^{\rm hf,(k-1,i)} : \mu \in \mathcal{P}_{\rm train}^{(k,i)}\}$

i.4. `if` $k > 1$, Parametric mesh adaptation $\quad \mathcal{S}^{(k-1,i)} \Rightarrow \mathcal{T}_{\rm hf}^{(k,i)}$

i.5. Registration $\quad \left(\mathcal{S}^{(k-1,i)}, \mathcal{T}_{\rm hf}^{(k,i)}\right) \Rightarrow \Phi^{(k,i)}$

i.6. MOR training $\quad \left(\Phi^{(k,i)}, \mathcal{T}_{\rm hf}^{(k,i)}\right) \Rightarrow \left(Z^{(k,i)}, \mathrm{ROM}^{(k,i)}\right)$

`EndFor`

7. Update the clusters if needed.

`EndFor`

Comments

To avoid communication between different meshes, we pursue a **hierarchical approach**: at each iteration, we split each element of the current partition (if necessary).

- Several off-the-shelves techniques can be employed for clustering.

Examples: (considered in the numerical experiments)

1. k-SVD. Aharon, Elad, Bruckstein, IEEE, 2006.
2. k-medoids based on (approximate) Wasserstein distance of GMMs.

   2.*a* GMMs are fit using the points obtained using the Ducros sensor.

   2.*b* Wasserstein distance is estimated as in [Chen et al., 2019] and [Delon&Desolneux, 2020].

The two methods lead to nearly-equivalent results for the model problem considered.

Comments

To avoid communication between different meshes, we pursue a **hierarchical approach**: at each iteration, we split each element of the current partition (if necessary).

- Several off-the-shelves techniques can be employed for clustering.

Examples: (considered in the numerical experiments)

1. k-SVD. Aharon, Elad, Bruckstein, IEEE, 2006.
2. k-medoids based on (approximate) Wasserstein distance of GMMs.

   2.*a* GMMs are fit using the points obtained using the Ducros sensor.

   2.*b* Wasserstein distance is estimated as in [Chen et al., 2019] and [Delon&Desolneux, 2020].

The two methods lead to nearly-equivalent results for the model problem considered.

- **Open question:** splitting criterion.

Current strategy: we split if the size of the current ROB is larger than $n_{\mathrm{thr}} = 25$.

Numerical results (I)

- We perform $N_{\mathrm{it}} = 4$ iterations of the adaptive procedure.
- We apply k-SVD: first, we set $\kappa = 3$; then, we set $\kappa = 2$.
- We consider anisotropic mesh refinement driven by the Hessian of the Mach field.

  F Alauzet, A Dervieux, P Frey, PL George,...
- MOR procedure and HF discretization are unchanged.

Numerical results (II): clustering

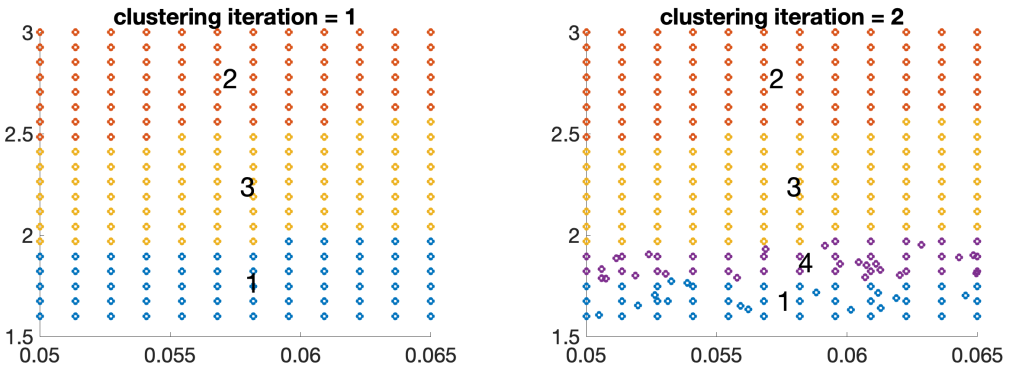

Numerical results (II): clustering

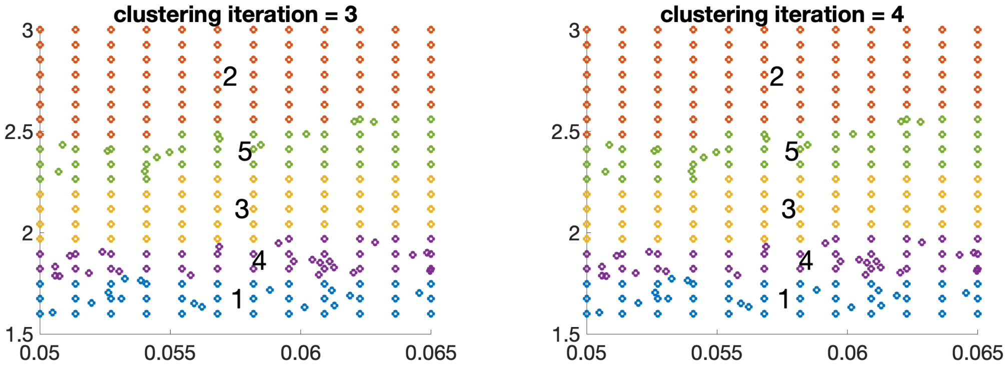

Interpretation: we have four distinct shock topologies; region 5 handles transition — which is difficult to capture through Lagrangian approximations.

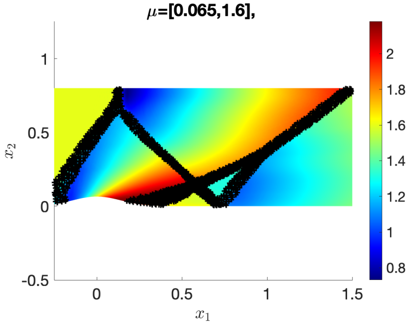

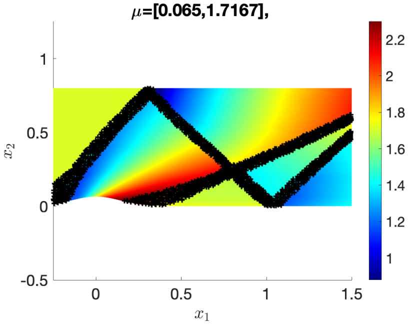

Numerical results (II): clustering

Interpretation: we have four distinct shock topologies; region 5 handles transition — which is difficult to capture through Lagrangian approximations.

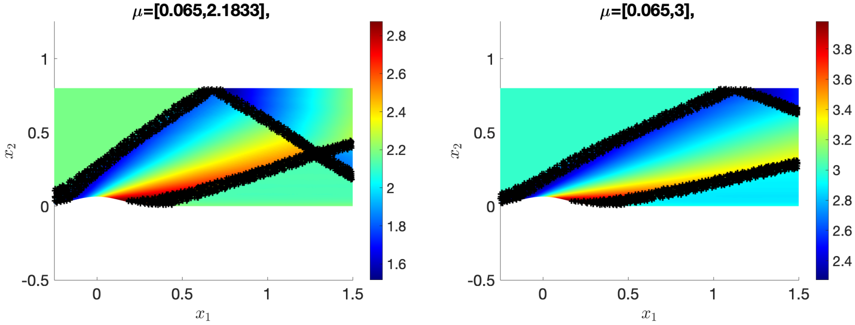

Numerical results (III): offline computational costs (total 12h 1')

Percentage of offline costs of the last greedy algorithms : $\approx 58\%$.

	it = 1	it = 2	it = 3	it = 4
nbr clusters:	3	4	5	5
ROB size:	22.67	21.00	20.00	21.00
mesh size:	1588.00	3035.00	5318.20	9290.40
initialization:	3262.04			
snapshot generation:	549.44	113.47	107.92	81.35
registration (sensor def.):	223.86	290.23	392.28	556.01
registration (optimization):	23.71	27.31	59.87	110.57
mesh adaptation:	0.00	2.69	5.73	11.94
clustering:		96.46	106.86	75.86
greedy alg (HF solves):	557.30	2145.59	7757.10	24233.01
greedy alg (overhead):	445.14	592.75	493.29	927.18

Linear-subspace projection-based model reduction

Preliminary (I): residual decomposition

Consider the FE mesh $\mathcal{T}_{\rm hf}$ of Ω with elements $\{\mathtt{D}_k\}_{k=1}^{N_{\rm e}}$, nodes $\{x_j^{\rm hf}\}_{j=1}^{N_{\rm v}}$ and facets $\{\mathtt{F}_j\}_{j=1}^{N_{\rm f}}$. The residual can be decomposed as follows:

$$\mathfrak{R}(u,v) = \sum_{k=1}^{N_{\rm e}} r_k^{\rm e}(u_k, v_k) + \sum_{j=1}^{N_{\rm f}} r_j^{\rm f}(u_j^+, u_j^-, v_j^+, v_j^-),$$

where $\{r_k^{\rm e}\}_k$ and $\{r_j^{\rm f}\}_j$ are local operators.

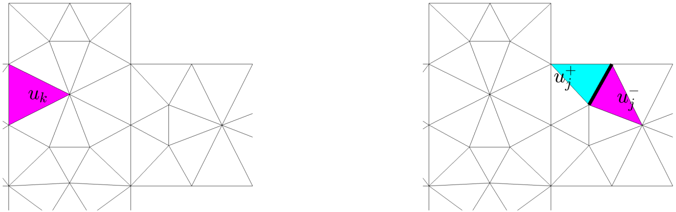

The decomposition is consistent with typical FE assembly routines.

Residual evaluation is accelerated by resorting to a reduced quadrature:

$$\mathfrak{R}_{\mu}^{\rm eq}(u,v) = \sum_{k=1}^{N_{\rm e}} \rho_k^{\rm e,eq} r_k^{\rm e}(u_k, v_k) + \sum_{j=1}^{N_{\rm f}} \rho_j^{\rm f,eq} r_j^{\rm f}(u_j^+, u_j^-, v_j^+, v_j^-),$$

where $\boldsymbol{\rho}^{\rm e,eq} \in \mathbb{R}_+^{N_{\rm e}}$, $\boldsymbol{\rho}^{\rm f,eq} \in \mathbb{R}_+^{N_{\rm f}}$ are sparse.

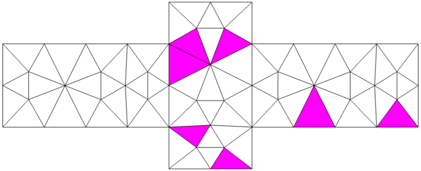

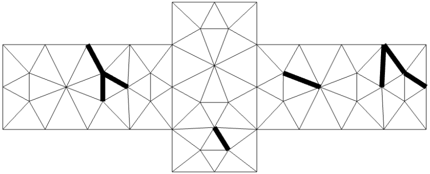

Refs: *reduced integration domain* (Ryckelynck, 2005); *mesh sampling and weighting* (Farhat et al., 2015); *empirical cubature* (Hernández et al., 2017); *empirical quadrature procedures* (Yano, Patera, 2019).

Remark: several alternatives are available (e.g., elementwise residual; pointwise residual).

Minimum residual formulation

We introduce the low-rank approximation: $\widehat{u}_\mu = \bar{u}_\mu + Z\widehat{\alpha}_\mu$.

- the offset $\bar{u}_\mu$ handles boundary conditions;
- the operator $Z = [\zeta_1, \ldots, \zeta_n] : \mathbb{R}^n \to \mathcal{X}$ is linear.

Our point of departure is the minimum residual formulation:

$$\min_{\alpha\in\mathbb{R}^n} \left(\sup_{v\in\mathcal{Y}} \frac{R_\mu(\bar{u}_\mu + Z\alpha, v)}{\|v\|_{\mathcal{Y}}} \right) = \min_{\alpha\in\mathbb{R}^n} \| \boldsymbol{Y}^{-1/2} \boldsymbol{R}_\mu (\bar{\boldsymbol{u}}_\mu + \boldsymbol{Z}\alpha) \|_2.$$

Refs: Maday et al., 2003; Yano, 2014 (*minimum residual MOR*); Grimberg et al., 2021 (*reduced quadrature rules*).

We introduce the low-rank approximation: $\widehat{u}_\mu = \bar{u}_\mu + Z\widehat{\alpha}_\mu$.

- the offset $\bar{u}_\mu$ handles boundary conditions;
- the operator $Z = [\zeta_1, \ldots, \zeta_n] : \mathbb{R}^n \to \mathcal{X}$ is linear.

Our point of departure is the minimum residual formulation:

$$\min_{\alpha \in \mathbb{R}^n} \left(\sup_{v \in \mathcal{Y}} \frac{R_\mu(\bar{u}_\mu + Z\alpha, v)}{\|v\|_{\mathcal{Y}}} \right) = \min_{\alpha \in \mathbb{R}^n} \| \boldsymbol{Y}^{-1/2} \boldsymbol{R}_\mu (\bar{\boldsymbol{u}}_\mu + \boldsymbol{Z}\alpha) \|_2.$$

- The ROM is online-efficient only for parametrically-affine problems.
- Application of reduced quadrature rules is possible if $\boldsymbol{Y}$ is diagonal.

Refs: Maday et al., 2003; Yano, 2014 (*minimum residual MOR*); Grimberg et al., 2021 (*reduced quadrature rules*).

Approximate minimum residual formulation ([TT, Zhang, 2021])

We introduce two approximations:

1. we replace $\sup_{v\in\mathcal{Y}}(\cdot)$ with $\sup_{v\in\mathcal{W}}(\cdot)$ where $\mathcal{W} = \mathrm{span}\{\psi_i\}_{i=1}^m$.

$$\min_{\alpha\in\mathbb{R}^n} \left(\sup_{v\in\mathcal{W}} \frac{R_\mu(\bar{u}_\mu + Z\alpha, v)}{\|v\|_\mathcal{Y}} \right) = \min_{\alpha\in\mathbb{R}^n} \|\boldsymbol{W}^\top \boldsymbol{R}_\mu(\bar{\boldsymbol{u}}_\mu + \boldsymbol{Z}\alpha)\|_2$$

Approximate minimum residual formulation ([TT, Zhang, 2021])

We introduce two approximations:

1. we replace $\sup_{v\in\mathcal{Y}}(\cdot)$ with $\sup_{v\in\mathcal{W}}(\cdot)$ where $\mathcal{W}=\mathrm{span}\{\psi_i\}_{i=1}^m$.

$$\min_{\alpha\in\mathbb{R}^n}\left(\sup_{v\in\mathcal{W}}\frac{R_\mu(\bar{u}_\mu+Z\alpha,v)}{\|v\|_{\mathcal{Y}}}\right)=\min_{\alpha\in\mathbb{R}^n}\|\boldsymbol{W}^\top\boldsymbol{R}_\mu(\bar{\boldsymbol{u}}_\mu+\boldsymbol{Z}\alpha)\|_2$$

2. we replace the HF residual with the weighted residual

$$\min_{\alpha\in\mathbb{R}^n}\|\boldsymbol{W}^\top\boldsymbol{R}_\mu^{\mathrm{eq}}(\bar{\boldsymbol{u}}_\mu+\boldsymbol{Z}\alpha)\|_2=\sum_{i=1}^m\left(R_\mu^{\mathrm{eq}}(\bar{u}_\mu+Z\alpha,\psi_i)\right)^2.$$

- The final ROM reads as a nonlinear least-square problem with m equations and n unknowns.
- The final ROM does not explicitly depend on $\boldsymbol{Y}$.

Notation:

- $\Phi : \Omega \times \mathcal{P} \to \mathbb{R}^d$ parametric diffeomorphism; $\{\Omega_\mu := \Phi_\mu(\Omega) : \mu \in \mathcal{P}\}$ family of parametric domains; $u_\mu : \Omega_\mu \to \mathbb{R}^D$ parametric solution; $\Phi_\mu(\mathcal{T}_{\rm hf})$ mesh with nodes $\{\Phi_\mu(x_j^{\rm hf})\}_j$ and elements $\{\mathtt{D}_{k,\mu}\}_k$.

Treatment of parameterized geometries (I)

Notation:

- $\Phi : \Omega \times \mathcal{P} \to \mathbb{R}^d$ parametric diffeomorphism; $\{\Omega_\mu := \Phi_\mu(\Omega) : \mu \in \mathcal{P}\}$ family of parametric domains; $u_\mu : \Omega_\mu \to \mathbb{R}^D$ parametric solution; $\Phi_\mu(\mathcal{T}_{\rm hf})$ mesh with nodes $\{\Phi_\mu(x_j^{\rm hf})\}_j$ and elements $\{\mathtt{D}_{k,\mu}\}_k$.

Two paradigms: TT, Zhang, CMAME, 2021

- Map-then-discretize (MtD): mesh fixed; PDE modified;
- Discretize-then-map (DtM): mesh modified; PDE fixed.

Example: Laplace: $-\Delta u = f, \; u|_{\partial \Phi_\mu(\Omega)} = 0$.

Define the empirical residual $\mathfrak{R}_\mu^{\rm eq}(u,v) = \sum_{k=1}^{N_{\rm e}} \rho_k^{\rm e,eq} r_k^{\rm e}(u,v)$.

MtD: $r_k^{\rm e}(u,v) = \int_{\mathtt{D}_k} \det(\nabla \Phi_\mu) \left(\nabla \Phi_\mu^{-1} \nabla \Phi_\mu^{-\top} \nabla u \cdot \nabla v - f \circ \Phi_\mu v \right).$

DtM: $r_k^{\rm e}(u,v) = \int_{\mathtt{D}_{k,\mu}} \nabla u \cdot \nabla v - fv \, dx$

Both approaches have been considered in the literature.

MtD: Rozza et al. 2008; Lassila, Rozza 2010.

DtM: Washabaugh et al. 2016; Dal Santo, Manzoni 2019.

MtD requires evaluation of Φ **and its derivatives** at quadrature points.

DtM requires to deform the nodes of sampled elements and facets $\Rightarrow$ much simpler to implement.

DtM requires *discrete bijectivity*: the deformed mesh with nodes $\{\Phi_\mu(x_j^{\mathrm{hf}})\}_j$ should not have inverted elements.

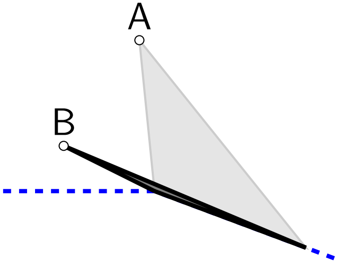

Treatment of geometric parameterizations influences convergence of the HF solver.

Example: Consider $-\partial_{xx} u = \sin(\pi x) \quad x \in \Omega = (0,1), \quad u|_{x=0,1} = 0.$

Let $\Phi : \Omega \to \Omega$ be piecewise-linear, and let $\mathcal{T}_{\mathrm{hf}}$ be a uniform grid with N_{e} elements of degree 3.

Apply MtD, iso-parametric DtM and sub-parametric DtM.

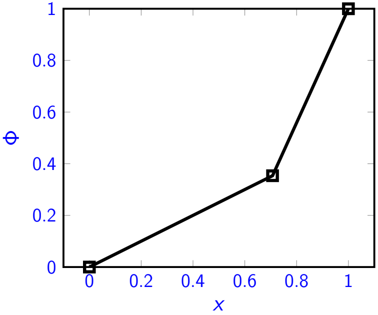

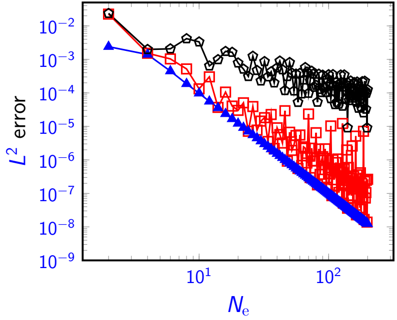

Treatment of geometric parameterizations influences convergence of the HF solver.

Example: Consider $-\partial_{xx} u = \sin(\pi x) \quad x \in \Omega = (0,1), \quad u|_{x=0,1} = 0.$

Let $\Phi : \Omega \to \Omega$ be piecewise-linear, and let $\mathcal{T}_{\mathrm{hf}}$ be a uniform grid with N_{e} elements of degree 3.

Apply MtD, iso-parametric DtM and sub-parametric DtM.

MtD fails to recover optimal rate.

DtM might have inverted elements.

DtM recovers optimal rate.